JOURNAL OF THERMOPHYSICS AND HEAT TRANSFER
Vol. 22, No. 1, January–March 2008

Full-Coverage Film Cooling for a Turbine Blade with Axial-Shaped Holes

Zhihong Gao,* Diganta P. Narzary,* Shantanu Mhetras,† and Je-Chin Han‡
Texas A&M University, College Station, Texas 77843-3123

DOI: 10.2514/1.31206

The film-cooling effectiveness on a fully film-cooled high pressure turbine blade is investigated using the pressure sensitive paint technique. Three rows of radial angled cylindrical holes are arranged in the showerhead region, while axial laid-back fan-shaped holes are provided on the blade surfaces with four rows on the pressure side and two rows on the suction side. The shaped holes are featured with 10° lateral expansion from the hole centerline and an additional 10° forward expansion to the blade surface. The coolant ejects through all the film-cooling holes at four average blowing ratios ranging from 0.3 to 1.2. The influence of wake from the upstream vane is simulated by placing a periodic set of rods upstream of the test blade. The freestream Reynolds number, based on the axial chord length and the exit velocity, is 750,000. The Mach numbers at the inlet and the exit are 0.27 and 0.44, respectively, resulting in a blade pressure ratio of 1.14. Results show the film-cooling effectiveness increases with increasing of the average blowing ratio. The presence of a stationary upstream wake can be very detrimental to the film effectiveness on the blade surface depending on the wake phase location. Compared with the case of no showerhead injection, the spanwise averaged film-cooling effectiveness in the downstream region of the pressure side and suction side rows increases with the showerhead injection. The film effectiveness on the pressure side is comparable to the compound angle-shaped holes and the axial-shaped holes, whereas on the suction side, the compound angle-shaped holes provide better effectiveness than the axial-shaped holes due to jet deflection and an expanded hole breakout area.

Nomenclature

A_c	=	film-cooling hole cross-section area of the cylindrical part
C_D	=	discharge coefficient
C_x	=	axial chord length (8.13 cm)
d	=	film-cooling hole diameter of the cylindrical part (0.65 mm)
H	=	blade height
M	=	average blowing ratio
M_{local}	=	local blowing ratio at hole row location
$\dot{m}_c$	=	coolant mass flow rate for a cavity
n	=	number of hole in a film-cooling row
P	=	static pressure on the blade surface
P_{O_2}	=	partial pressure of oxygen
P_t	=	total pressure upstream of the blades, Pa
$P_{t,\text{cavity}}$	=	total pressure inside a coolant cavity, Pa
R	=	gas constant for air (287 J/Kg · K)
r	=	number of film-cooling rows in a coolant cavity
s	=	distance between adjacent holes in a hole row (5.3 mm)
T_c	=	coolant temperature, °C
T_f	=	local film temperature, °C
T_m	=	mainstream temperature, °C
V_c	=	average velocity of coolant from the film-cooling holes in the hole row location, m/s
$V_{c,\text{local}}$	=	actual velocity of coolant from the film-cooling holes in the hole row location, m/s
V_m	=	local mainstream velocity at the hole row location, m/s
x	=	axial distance from blade leading edge, cm
y	=	distance along blade span measured from hub
α	=	film-cooling hole inclined angle to the surface
β	=	film-cooling hole inclined angle to the streamwise direction
γ	=	lateral expansion angle from the centerline of a film-cooling hole
δ	=	film-cooling hole forward expansion angle to the surface
η	=	local film-cooling effectiveness
$\bar{\eta}$	=	spanwise-averaged film-cooling effectiveness
ρ_c	=	density of coolant air, kg/m^3
ρ_m	=	density of mainstream air, kg/m^3

Subscripts

air	=	mainstream air with air as coolant
blk	=	image without illumination (black)
mix	=	mainstream air with nitrogen as coolant
ref	=	reference image with no mainstream and coolant flow

Presented as Paper 4031 at the 39th AIAA Thermophysics Conference, Miami, FL, 25–28 June 2007; received 22 March 2007; revision received 15 June 2007; accepted for publication 19 June 2007.

*Research Assistant, Turbine Heat Transfer Laboratory, Department of Mechanical Engineering.

†Research Assistant, Turbine Heat Transfer Laboratory, Department of Mechanical Engineering; currently Senior Engineer, Siemens Power Company, Orlando, FL.

‡Distinguished Professor and Holder of Marcus Easterling Chair, Turbine Heat Transfer Laboratory, Department of Mechanical Engineering; jc-han@tamu.edu. Associate Fellow AIAA.

Introduction

THE ability of today's gas turbine engines to withstand increasingly higher turbine-inlet temperatures has been largely due to the advancement in cooling technology. One of the commonly used cooling techniques in modern high pressure and high temperature gas turbine engines is film cooling. Among the variety of film-cooling hole designs, four hole geometries are generally considered: cylindrical holes, laterally diffused (fan shaped) holes, forward-diffused (laid-back) holes, and laterally and forward-diffused (laid-back fan shaped) holes. Figure 1 schematically shows the hole geometries with the cross-section view cutting along the hole centerline. Depending on the angle (β) of the projected hole centerline on the surface with respect to the mainstream direction, a film-cooling hole can be identified as an axial hole (if $\beta = 0$ deg) or a compound angle (CA) hole (if $\beta > 0$ deg). Figure 1 also

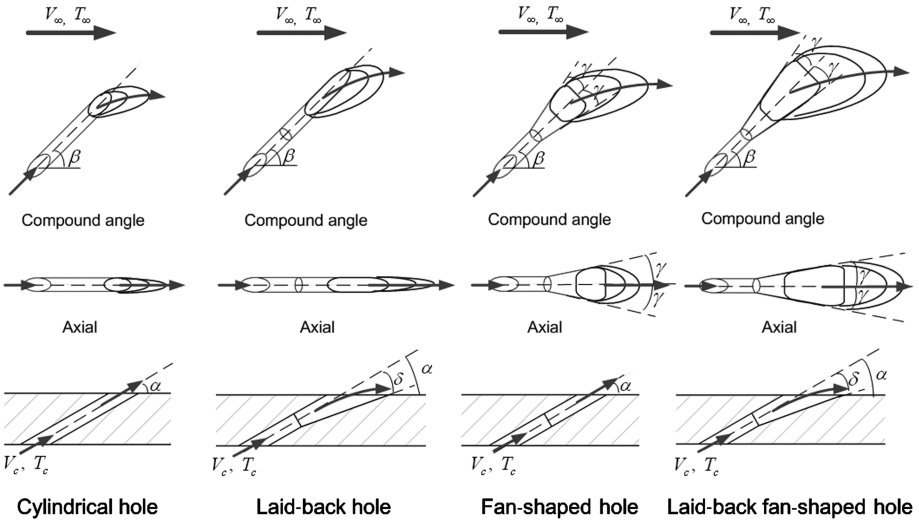

Fig. 1 Film-cooling hole configurations.

conceptually shows the film-cooling effectiveness distribution produced by the various hole configurations. In general, the compound angle hole gives better effectiveness as the coolant is deflected by the mainstream and covers a wider surface area. The shaped holes perform better than the cylindrical holes because the expanded hole breakout area reduces the jet momentum and diminishes the jet liftoff.

Many researchers quantitatively assessed two or more film-cooling hole configurations on a flat plate with axial holes. Goldstein et al. [1] compared film-cooling effectiveness for straight round holes and axial fan-shaped holes with lateral diffusion of 10°. They reported a significant increase in the film-cooling effectiveness immediately downstream of the shaped holes as well as increased lateral coolant coverage. Thole et al. [2] carried out flowfield measurements using laser Doppler velocimetry (LDV) at the exit of three different hole geometries. The hole geometries included a cylindrical hole, a fan-shaped hole, and a laid-back hole. Their findings showed that both the shaped holes had less shear mixing of the injection jet with the mainstream and greater lateral spreading of the coolant compared to that of a round hole. Additionally, the laid-back hole had relatively lower film effectiveness than the fan-shaped hole due to excessive diffusion of the coolant and subsequent mainstream interaction. Gritsch et al. [3] studied the same cooling hole configurations and orientations as [2] with a density ratio of 1.85. As compared to the cylindrical hole, both shaped holes showed significantly improved thermal protection of the surface downstream of the ejection location, particularly at high blowing ratios. Along similar lines, Yu et al. [4] studied film-cooling effectiveness and heat transfer distributions on a flat plate with a cylindrical hole, a laid-back hole, and a laid-back fan-shaped hole. The laid-back fan-shaped hole provided the highest film-cooling performance as well as overall heat transfer reduction.

All of the above studies were performed on a flat plate with axially oriented holes. Schmidt et al. [5] examined a film-cooling performance of 60 deg compound angled holes on a flat plate surface, with and without a forward expanded shaped exit, and compared that with axial cylindrical holes. Both compound angle holes had significantly greater effectiveness at larger momentum flux ratios. The compound angle holes with expanded exits had a much improved lateral distribution of coolant near the hole for all momentum flux ratios. Dittmar et al. [6], in a slight deviation, conducted measurements on a model of a suction side of an actual turbine guide vane inside a wind tunnel. Four different cooling hole configurations were investigated: a double row of cylindrical holes, a double row of discrete slots, a single row of axial fan-shaped holes, and a single row of compound angle fan-shaped holes. The streamwise injection angle α was 45 deg for all cases with an additional lateral angle β of 35 deg from the mainstream direction for compound shaped holes. According to their study, fan-shaped holes provided good effectiveness values at moderate and high blowing ratios unlike the cylindrical holes which suffered from jet separation. In another study involving pressure and suction side models inside a wind tunnel, Chen et al. [7] investigated both axial and compound angle laid-back fan-shaped holes. The compound angle β in their study was 45 deg. On the concave surface, improvement in laterally averaged effectiveness due to the addition of a compound angle was found at a high blowing ratio of 2. On the convex surface, significant improvement in effectiveness was seen at both low and high blowing ratios.

Hole shape studies in linear cascades are fewer in comparison to those in flat plate and model airfoils. Teng and Han [8] studied one row of film holes near the gill-hole portion of the suction side. The hole geometries considered in their study were the same as those of [2,3] but with a slightly higher inclined angle α of 40 deg. They reported that spanwise-averaged film effectiveness of shaped holes could be about 2 times higher than that of cylindrical holes. In addition, fan-shaped holes performed better than laid-back fan-shaped holes.

The effect of unsteady wake on film-cooling effectiveness and coolant jet temperature profiles on the suction side of a turbine blade were investigated by Teng et al. [9] and in a low speed cascade. A spoked-wheel mechanism was used to generate the upstream wakes. They found that unsteady wake reduced the effectiveness magnitudes. Local heat transfer immediately downstream of the holes was found to increase by as much as 60% due to film injection. Ou et al. [10] simulated unsteady wake conditions using the same mechanism as Teng et al. [9]. They tested a no-wake case and wake Strouhal numbers of 0.1 and 0.3. Air and CO_2 were used to simulate the effect of the density ratio. They found that the additional increases in Nusselt numbers due to unsteady wake and density ratio were only secondary when compared to the dramatic increases in Nusselt numbers only due to film injection over the no film-cooling case. Furthermore, Mehendale et al. [11], in the same test facility and for the same experimental conditions, found that an increase in the wake Strouhal number led to a decrease in film effectiveness over most of the blade surface for both density ratio injections and at all blowing ratios. Du et al. [12] performed a similar experiment with the addition of trailing edge coolant ejection from the wake-producing bars. The addition of wake coolant had a relatively small effect on the downstream blade heat transfer coefficient, but reduced leading edge film effectiveness below the wake case with no coolant ejection. Detailed heat transfer measurements on a transonic film-cooled blade with and without nozzle guide vane (NGV) shock waves and wakes were made by Rigby et al. [13]. It was found that there was a significant change of film-cooling behavior on the suction surface when simulated NGV unsteady effects were introduced. Heidmann et al. [14] studied the effect of wake passing on a showerhead film-cooling performance in an annular cascade with an upstream rotating

row of cylindrical rods. A high wake Strouhal number was found to decrease effectiveness but it was also found to divert the coolant toward the pressure side resulting in slightly better cooling on the pressure side.

Most of the experimental studies of the blade film cooling were focused on the midspan region only. By using the pressure sensitive paint (PSP) techniques, Mhetras and Han [15] recently obtained a detailed film-cooling effectiveness distribution on a fully film-cooled blade surface including showerhead blowing. Radial angled cylindrical holes were used in the showerhead region, while the compound angle cylindrical holes were used on the blade surface. The highest effectiveness on the blade surface was obtained at $M = 0.9$ with the compound angled cylindrical holes. Keeping the same showerhead film hole design and changing the hole geometry on the pressure side and suction side, Narzary et al. [16] measured the film-cooling effectiveness distribution with compound angle laid-back fan-shaped holes on the blade surface. Their results showed that the compound angle-shaped holes provide higher film-cooling effectiveness than the compound angle cylindrical holes. The film-cooling effectiveness for the compound angle-shaped holes increased with the increasing of the blowing ratio and no optimal blowing ratio was observed at $M = 0.3$–1.2. More recently, Gao et al. [17] studied a film-cooling effectiveness distribution on the blade pressure side or suction side with an axial-shaped hole without showerhead film cooling. Their results showed that the moderate blowing ratios $M = 0.6$–1.2 gave better film-cooling effectiveness. By further increasing the blowing ratio to $M = 1.5$, the effectiveness decreased due to jet liftoff.

It is known that the compound angle cylindrical holes provide higher film-cooling effectiveness as well as higher heat transfer coefficients and losses as compared to the axial angle cylindrical holes. Similarly, it is expected that the compound angle-shaped holes would provide higher film-cooling effectiveness as well as higher heat transfer coefficients and losses as compared to the axial angle-shaped holes. However, it is unclear, on a one-to-one basis, how much difference there is in film-cooling effectiveness between the two types of shaped hole designs in the cascade environment. This current study is focused on blade film cooling with axial angle-shaped holes, which are commonly used in modern high pressure and high temperature gas turbine blades. Four rows of axial-shaped holes are distributed on the pressure side, with two such rows on the suction side. The effect of showerhead film cooling on the blade surface film cooling is included. The showerhead film-cooling design consists of three rows of radial angled cylindrical holes. The film-cooling effectiveness on the blade surface is measured using the PSP technique. The upstream wake effect is simulated by placing a stationary rod at different phase locations upstream of the blades along the pitchwise direction.

Experimental Setup

The measurements were conducted in a five-blade linear cascade facility as shown in Fig. 2. The inlet cross section of the test section was 19.6 cm (width) × 12.7 cm (height), whereas the exit cross section was 12.9 cm (width) × 12.7 cm (height). The top plate, which acted as the shroud for the blades, and the outer side walls of the test section were machined out of 1.27-cm thick acrylic sheets for optical access. Images of the test surface were captured by a 12-bit, scientific grade charge-coupled device (CCD) camera. The mainstream air was supplied by a centrifugal compressor that can deliver a volume flow rate up to 6.2 m^3/s. A honeycomb mesh, 7.62 cm long with a cell size of 1.27 cm, was put 1.78 m upstream to the blade leading edge to uniform the flow. Downstream flow periodicity was ensured by adjusting the cascade tailboards. The cascade inlet and exit velocities were set to be 96 and 156 m/s corresponding to inlet and exit Mach numbers of 0.27 and 0.44, respectively. The Reynolds number based on the axial chord length and exit velocity was 750,000 and the overall pressure ratio (P_t/P) was 1.14 (where P_t is inlet total pressure and P is exit static pressure). Turbulence intensity and boundary layer thickness was recorded 6.3 cm upstream of the middle blade. A turbulence intensity of 2% was measured in the middle of the channel, and the boundary layer thickness was about 25 mm.

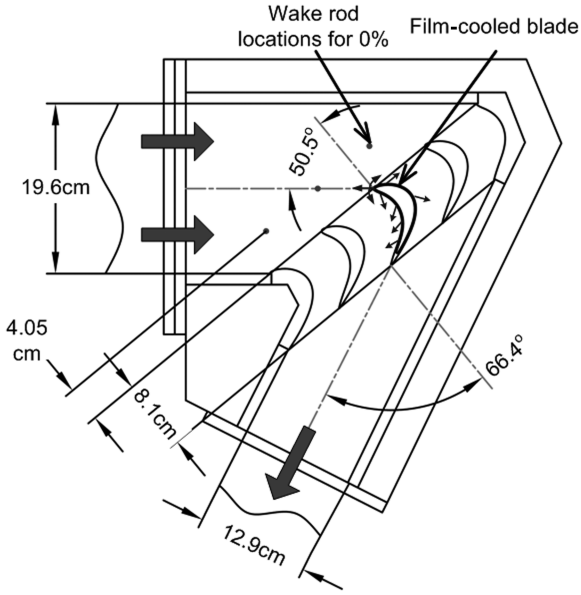

Fig. 2 Schematic of the cascade with a film-cooled blade.

All five blades in the cascade had a span of 12.64 cm and an axial chord length of 8.13 cm. The leading edge of the blades could be approximated as an arc with a radius of 2.4 mm. The test blade, placed in the middle of the cascade, was made of stereolithography (SLA). It had a squealer tip with a recess of 2.4% of blade span (2.84 mm) while the two adjacent blades had a flat tip. Figure 3 shows the film-cooling design and the internal coolant supply passages on the test blade. Three rows of showerhead film-cooling holes were angled (α) 30 deg to the blade surface. The middle row (SH-ST) was aligned with the stagnation line while the other two rows (SH-PS, SH-SS) were placed 15 deg apart on either side. Twenty-two cylindrical holes with a diameter of 0.65 mm were drilled in each showerhead row resulting in a hole-to-hole spacing of 5.3 mm ($s/d = 8.2$) and hole length-to-diameter ratio (L/d) of 12.7. Axial laid-back fan-shaped holes were used on the pressure surface and suction surface. Four rows are on the pressure side at axial locations of 1.24 cm (PS1, 23 holes), 3.62 cm (PS2, 22 holes), 5.01 cm (PS3, 23 holes), and 6.1 cm (PS4, 22 holes). Two rows were provided on the suction side at axial locations of 0.38 cm (SS1, 23 holes) and 3.56 cm (SS2, 22 holes). The holes in adjacent rows were staggered with respect to each other. Because of the staggered arrangement, rows PS2, PS4, and SS2 have one hole less than the other rows. The hole-to-hole spacing, however, was maintained at $8.2d$. The shaped holes had a lateral expansion angle γ of 10 deg from the hole centerline and a forward expansion angle δ of 10 deg to the blade surface. The total length of the hole was 6.8 times of the hole diameter of the cylindrical part (0.65 mm). The shaped hole expansion started at $3.9d$, which resulted in a area ratio of 3.7 between the hole exit cross-section area to metering part (cylindrical part) cross-section area. Coolant was supplied to all the film hole rows via four cavities as labeled from 1 to 4 in Fig. 3. The first cavity near the leading edge was designed to supply coolant to the showerhead rows as well as rows PS1 and SS1. The second cavity was shared by rows PS2 and SS2. The remaining two cavities supplied coolant to rows PS3 and PS4, respectively. The cavity cross sections were modeled similar to the internal cooling passages in turbine blades with coolant injection through the bottom of the blade.

Metal rods were inserted periodically upstream of the blades to simulate the wakes generated by the upstream vanes at different phase locations. A rod diameter of 4.8 mm was selected to model a typical airfoil trailing edge. The rods were located at a distance equivalent to 50% of the axial chord (4 cm) upstream of the blades. They were placed at four equally spaced intervals corresponding to the blade pitch. The rod directly upstream of the leading edge was

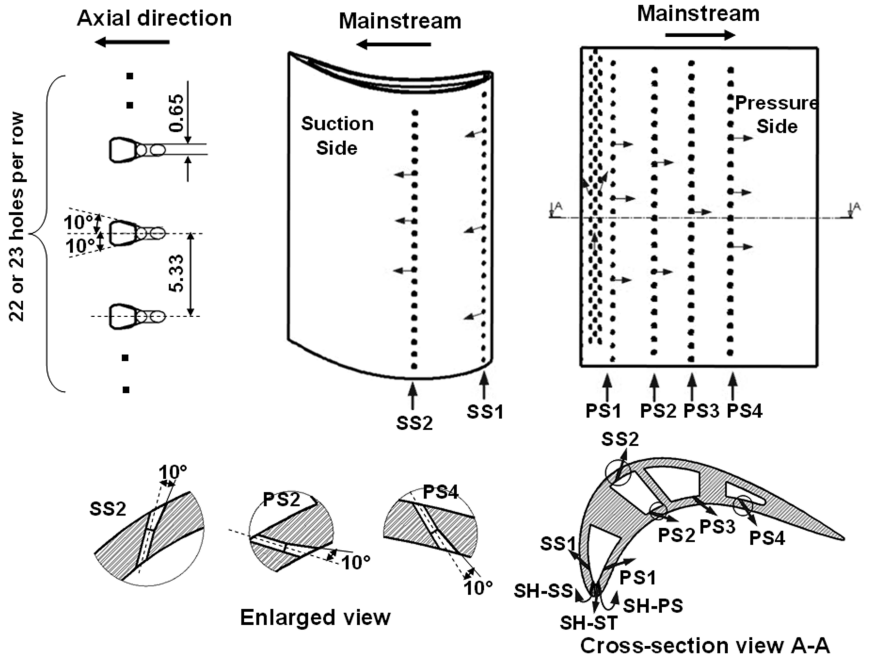

Fig. 3 Film-cooling hole design on the test blade.

indicated as the 0% phase location and was 6.3 cm upstream of the leading edge in the flow direction. Rod locations for 25, 50, and 75% were progressively located along the blade pitchwise direction as indicated in Fig. 4. The periodically placed upstream rods may be thought of as a progressing wake in a rotating turbine. Four sets of experiments were conducted to cover all phase locations. Two rods were placed with one in the pressure side passage of the test blade and the other at the corresponding periodic location in the suction side passage for phase locations of 25, 50, and 75%; whereas for phase location 0%, a single rod was placed in front of the stagnation point of the center test blade. The traveling path of wakes generated by the rods at different phases is also conceptually shown in Fig. 4.

Film-Cooling Effectiveness Measurement Theory and Data Analysis

Data for film-cooling effectiveness were obtained using the PSP technique. PSP is a photoluminescent material that emits light when excited, with the emitted light intensity inversely proportional to the partial pressure of oxygen. This light intensity is recorded using a CCD camera. Details of using PSP for pressure measurements are given by McLachlan and Bell [18]. The image intensity recorded by the camera during data acquisition is normalized with a reference image intensity (I_{ref}) taken under no-flow conditions. Background noise in the optical setup is removed by subtracting the image intensities with the image intensity obtained under no-flow conditions and without light excitation (I_{blk}). The resulting intensity ratio can be converted to a pressure ratio using a predetermined calibration curve and can be expressed as

$$\frac{I_{\text{ref}} - I_{\text{blk}}}{I - I_{\text{blk}}} = f\left(\frac{(P_{O_2})_{\text{air}}}{(P_{O_2})_{\text{ref}}}\right) = f(P_{\text{ratio}}) \tag{1}$$

where I denotes the intensity obtained for each pixel and $f(P_{\text{ratio}})$ is the relationship between intensity ratio and pressure ratio obtained after calibration.

Calibration of the PSP system was performed using a vacuum chamber at several known pressures varying from 0 to 1.8 atm. The same optical setup that was used during experiments was chosen for calibration. The calibration curve is shown in Fig. 5. PSP is also sensitive to temperature with higher temperatures resulting in lower light emission. Hence, the paint was also calibrated at different temperatures. It was observed that if the emitted light intensity at a certain temperature was normalized with the reference image intensity taken at the same temperature, the temperature sensitivity can be minimized as shown in Fig. 5b. Hence, during experiments, the reference I_{ref} and black I_{blk} images were acquired immediately after stopping the mainstream flow so that the test blade surface temperature does not change appreciably.

To obtain film-cooling effectiveness, air and nitrogen were used alternately as a coolant. Nitrogen which has nearly the same molecular weight as that of air displaces the oxygen molecules on the

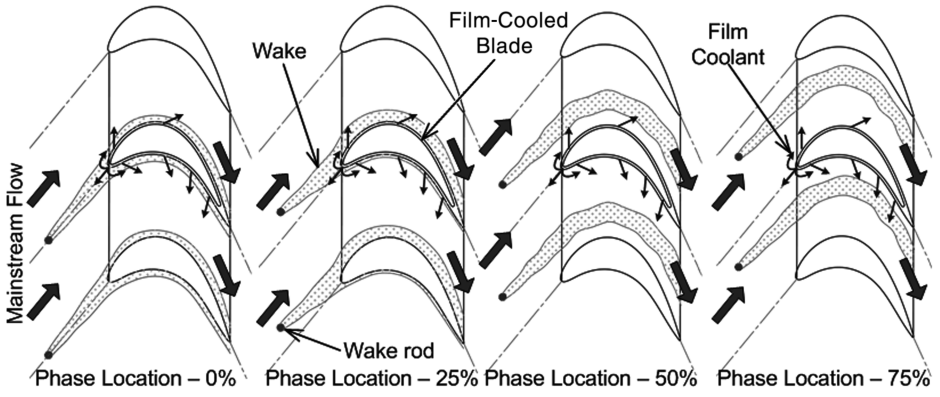

Fig. 4 Wake rod phase locations and conceptual view of the wake effect on the test blade.

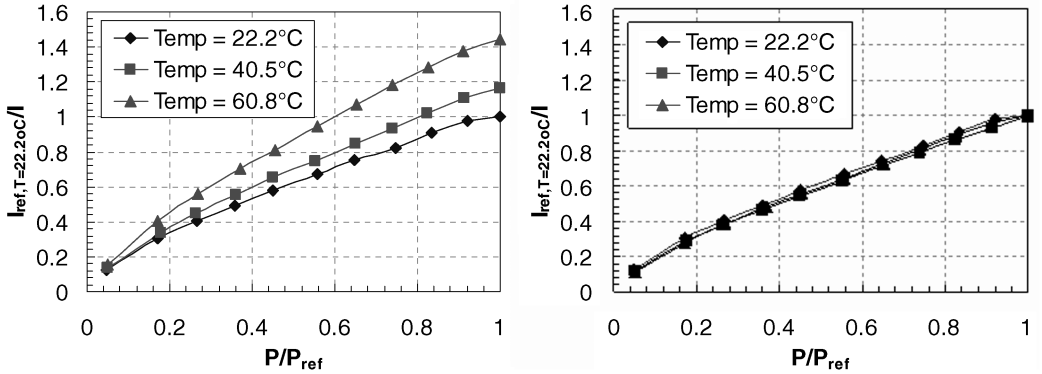

Fig. 5 a) PSP calibration at single reference temperature; b) PSP calibration at corresponding reference temperature.

surface causing a change in the emitted light intensity from PSP. By noting the difference in partial pressure between the air and nitrogen injection cases, the film-cooling effectiveness can be determined using the following equation:

$$\eta = \frac{C_{\text{mix}} - C_{\text{air}}}{C_{N_2} - C_{\text{air}}} = \frac{C_{\text{air}} - C_{\text{mix}}}{C_{\text{air}}} = \frac{(P_{O_2})_{\text{air}} - (P_{O_2})_{\text{mix}}}{(P_{O_2})_{\text{air}}} \tag{2}$$

where C_{air}, C_{mix}, and C_{N_2} are the oxygen concentrations of mainstream air, air/nitrogen mixture, and nitrogen on the test surface, respectively. The definition of film effectiveness in Eq. (2) based on mass transfer analogy assumes a similar form as that of adiabatic film-cooling effectiveness given in Eq. (3):

$$\eta = \frac{T_{\text{mix}} - T_m}{T_c - T_m} \tag{3}$$

The accuracy of the PSP technique for measuring film-cooling effectiveness has been compared by Wright et al. [19] on a flat plate with compound angled film holes using a steady-state infrared (IR) technique and a steady-state temperature sensitive paint (TSP) technique. Results were obtained for a range of blowing ratios and show reasonable agreement with each other. All three measurement techniques agreed within 15% of each other. Larger uncertainties for heat transfer techniques such as IR and TSP methods were due to lateral heat conduction in the flat plate as corrections for heat conduction were not included in the presented results.

The test blade with film-cooling holes was coated with PSP using an air brush. It was excited by a strobe light fitted with a narrow bandpass interference filter (optical wavelength = 520 nm). A flexible dual fiber optic guide was used to get a uniform incident light distribution on the test surface. Upon excitation, the PSP coated surface emitted light with a wavelength higher than 600 nm. A 12-bit scientific grade CCD camera (Cooke Sensicam QE with CCD temperature maintained at −15°C using a two-stage peltier cooler), fitted with a 35 mm lens and a 600 nm long-pass filter, recorded images. The filter mounted on the camera was chosen such that it did not allow any reflected light from the illumination source to pass through. A schematic of the optical component setup and camera positions is depicted in Fig. 6. Because of the blade curvature, images were captured at five camera positions: two positions for the pressure side and three for the suction side. The camera and the strobe light were triggered simultaneously using a transistor–transistor logic (TTL) signal from a function generator. A total of 200 tagged image file (TIF) images were captured and ensemble averaged to get the individual intensities. The spatial resolution of each image was 0.6 mm/pixel. A computer program was used to convert these pixel intensities into pressure using the calibration curve and then into film-cooling effectiveness. The coolant flow rate into each cavity was set using a rotameter based on prior calculation for the desired blowing ratio. The coolant was heated to the same temperature as mainstream air (∼35°C) before supplying through the holes.

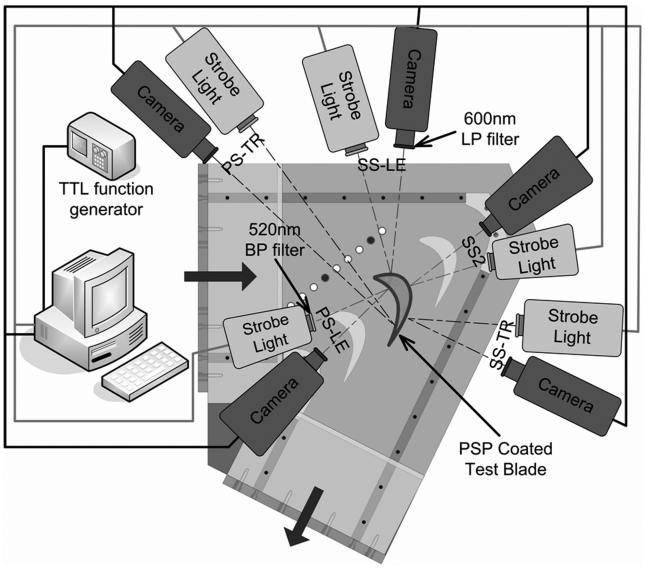

Fig. 6 Optical component setup.

Uncertainty calculations were performed based on a confidence level of 95% and are based on the uncertainty analysis method of Coleman and Steele [20]. Lower effectiveness magnitudes have higher uncertainties. For an effectiveness magnitude of 0.3, uncertainty was around ±1%, whereas for an effectiveness magnitude of 0.05, uncertainty was as high as ±8%. This uncertainty is the result of uncertainties in calibration (4%), image capture (1%), and blowing ratio (4%).

Flow and Local Blowing Ratio Distribution on the Blade Surface

Figure 7 shows the Mach number distributions at three span locations −50, 75, and 94% without the presence of wake rods and film-cooling holes. The Mach numbers were calculated from the pressure ratio P_t/P, which was obtained by normalizing the cascade inlet total pressure P_t with the static pressure P on the blade surface. The static pressure on the blade surface was measured using pressure taps instrumented on a separate blade. The inlet total pressure was measured using a pitot tube placed 6.3 cm upstream of the center blade. The pressures were recorded with a 48-channel scanivalve system coupled with LabView software. LabView discarded all data that fell outside the initial mean ±1.5 standard deviation. It then recorded the mean value of the screened data. Every pressure measurement was repeated at least 3 times to reduce data uncertainty and verify data repeatability. The pressure side Mach number distributions for all three span locations are more or less similar. There is a gradual decrease in the Mach number till $x/C_x \sim 0.6$, after

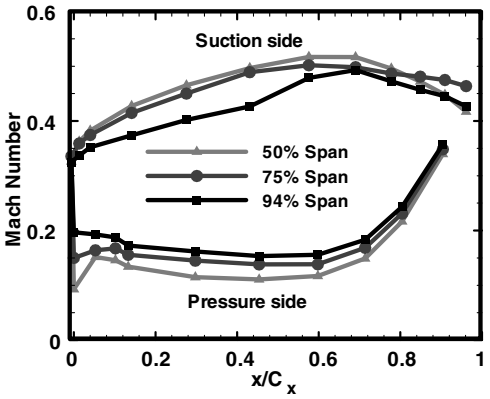

Fig. 7 Mach number distributions without upstream wake.

which there is a sharp rise. On the suction side, the Mach number distribution shows a steady increase till $x/C_x \sim 0.65$, beyond which it starts falling. The point of inflection on the suction side corresponds to the throat region where the mainstream reaches its maximum velocity. The interaction of the mainstream and tip leakage vortex can be clearly observed from this plot, with an appreciable reduction of Mach number for the 94% span case in the first half of the blade axial chord.

Figure 8 shows the Mach number distribution under the influence of stationary wakes at all phase locations. The data are presented for the same three blade span locations. It is interesting to find that the midspan region is most affected by the upstream rods followed by 75 and 94% of span locations. This is indicative of the fact that the strong endwall vortices and tip leakage vortices override the disturbance created by the wake rods. In the midspan region, the influence of endwall vortices is negligible; the effect of wake rods becomes evident. It has to be noted that the pressure measurements were carried out on a blade without cooling holes. With the presence of film cooling, the boundary layer attached to the blade surface is disturbed. This is particularly true at higher blowing ratios. In general, on the pressure side, the wake rods at phase 0% show the highest influence on the Mach number distribution followed by phase 75%. The other two wake rod phases show little or no effect. On the suction side, rod phase 25% followed by rod phase 0% shows the highest influence in the midspan region. This agrees well with the conceptual wake paths depicted in Fig. 4. On the suction side near the tip region (75 and 94% blade span), the wake rod effect on the Mach number is not substantial as the endwall secondary flow is predominant.

Experiments were performed at four average blowing ratios (M) of 0.3, 0.6, 0.9, and 1.2. The average blowing ratio was defined as $M = \rho_c V_c / \rho_m V_m$, where V_m is mainstream velocity at 50% of the blade span in the hole row location calculated from P_t/P. The total pressure P_t was measured using a pitot tube probe upstream of the test blade and static pressure was measured through surface taps along a blade without the film injection. By knowing the local mainstream velocity, the coolant mass flow rate required by a coolant cavity ($\dot{m}_c$) for a given average blowing ratio was predetermined by

$$\dot{m}_c = \sum_{k=1}^{r} n \cdot M \rho_m V_m A_c \tag{4}$$

where $r = 5$, 2, 1, amd 1 for the first, second, third, and fourth cavities, respectively. The coolant mass flow rate was set using a dedicated rotameter connected to the coolant loop for each cavity. In the real test, the coolant mass flux from each row is dependent on the pressure differential across the hole and hole geometry. Hence, the actual or local blowing ratio $M_{\text{local}} = \rho_c V_{c,\text{local}} / \rho_m V_m$ for the rows in the first and second cavities can be deviated away from the average blowing ratio M due to the variation mainstream velocity and the outer pressure on the blade surface. To check the coolant distribution, the row-based local blowing ratio was examined. The discharge coefficients C_D, as discussed by Gritsch et al. [21], was calculated by

$$\dot{m}_c = \sum_{k=1}^{r} C_D \cdot \left(\frac{\pi}{4} d^2\right) \cdot n \left[P_{t,\text{cavity}} \left(\frac{P}{P_{t,\text{cavity}}}\right)^{\frac{\gamma+1}{2\gamma}} \right] \sqrt{\frac{2\gamma}{(\gamma-1)RT_c} \left[\left(\frac{P_{t,\text{cavity}}}{P}\right)^{\frac{\gamma-1}{\gamma}} - 1 \right]} \tag{5}$$

The discharge coefficient C_D was assumed constant for all the holes in the same cavity for a given average M. It should be noted that the constant assumption of C_D for all holes in the cavity may not be true as C_D depends on not only the geometry but also the external and internal flow conditions. It was assumed that the deviation in the discharge coefficients from hole to hole is not significant and hence an average value can be assumed without introducing a significant error. Once the C_D for a given M was determined, the actual (or local) blowing ratio for a particular row was estimated. Figure 9 shows the row-based local blowing ratio distribution. Although the high outer pressure causes less coolant ejection from the showerhead stagnation row (SH-ST), the very low mainstream velocity results in substantial high local blowing ratios for the SH-ST row. Similarly, the local blowing ratio on the pressure side rows is higher than its suction surface counterparts except $M = 0.3$ in cavity 2. Although more coolant injects to the low-pressure suction surface, the mainstream velocity on the suction surface is much higher than that on the pressure side. This results in a lower local blowing ratio on the suction side. This local blowing ratio distribution will affect the film-cooling effectiveness distribution, which will be seen in the next section.

Film-Cooling Effectiveness on the Blade Surface

The effectiveness data obtained at each individual camera position were projected onto a radial plane passing through the axial chord of the blade and formed a complete picture for the pressure side or the suction side of the blade. In the contour plots, the abscissa and the ordinate were normalized with the axial chord length and the blade height, respectively.

Film-cooling effectiveness distributions on the blade surface was measured at four different average blowing ratios and four wake rod positions using the pressure sensitive paint technique. To study the

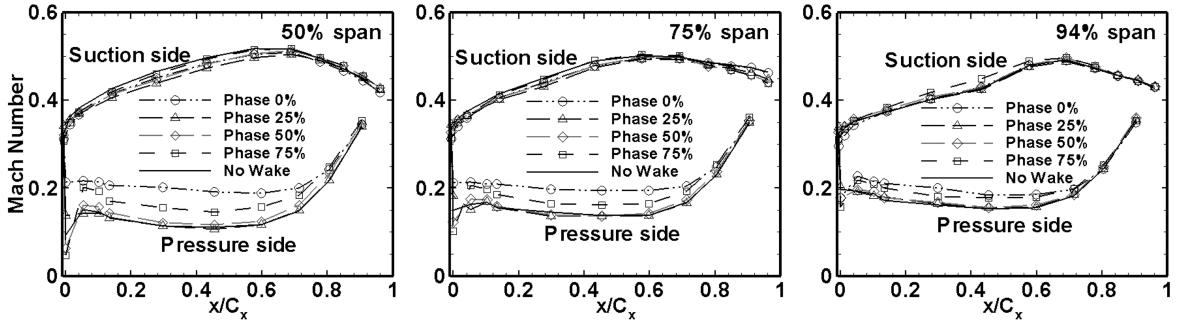

Fig. 8 Mach number distributions under the influence of upstream wake rods.

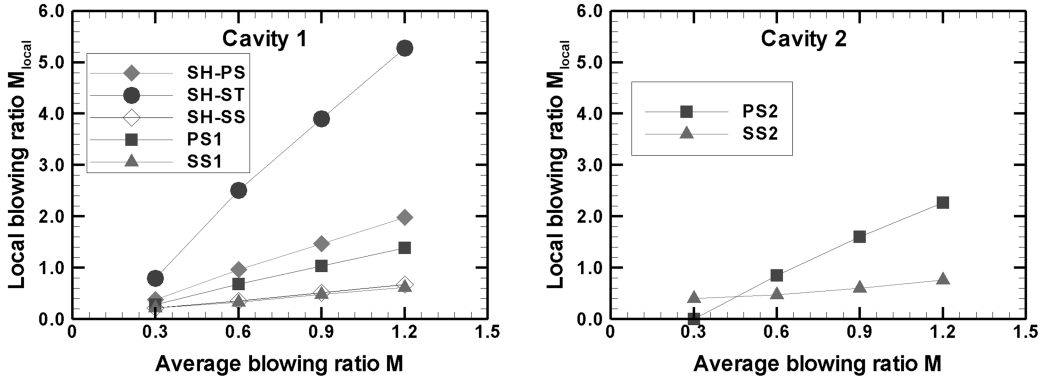

Fig. 9 Local blowing ratio distributions.

effect of upstream wake, the film-cooling effectiveness without the presence of the wake rods was taken as a baseline case. Figure 10 shows the film-cooling effectiveness distribution on the blade surface for the baseline case (without placement of upstream rods). The coolant jets from the axial shaped holes are redirected by the mainstream. The tip leakage flow drives the coolant upward toward the tip on the pressure side near the tip region, while the pressure side horseshoe vortex and corner vortex drag the coolant to the hub on the pressure side near the hub region. Starting at $x/C_x \sim 0.3$ on the suction side, the coolant is swept toward the midspan by the spiraling motion of the passage vortex and the tip leakage vortex. These vortices result in two unprotected triangular zones near the tip and hub on the suction surface. The effects of secondary vortices on the effectiveness distribution were also observed in [15–17].

It can be seen from the contour plots that the film-cooling effectiveness increases with the average blowing ratio on both the pressure side and the suction side. At the lowest average blowing ratio $M = 0.3$, the pressure inside cavity 1 is relatively low. The high outer pressure on the pressure side and showerhead region prohibits the coolant ejecting from PS1 and showerhead rows. As a result, most of the coolant is released from SS1 holes to the suction side where pressure is relatively low. For the second shared cavity at $M = 0.3$ and $M = 0.6$, similarly, little coolant is ejected from the PS2 row and most of the coolant is diverted to SS2 rows. This leaves a large area on the pressure surface uncooled. The mainstream ingestion may also occur to the holes where the coolant ejection does not show up. When the internal pressure inside the cavity increases with the average blowing ratio, the coolant is able to eject from the

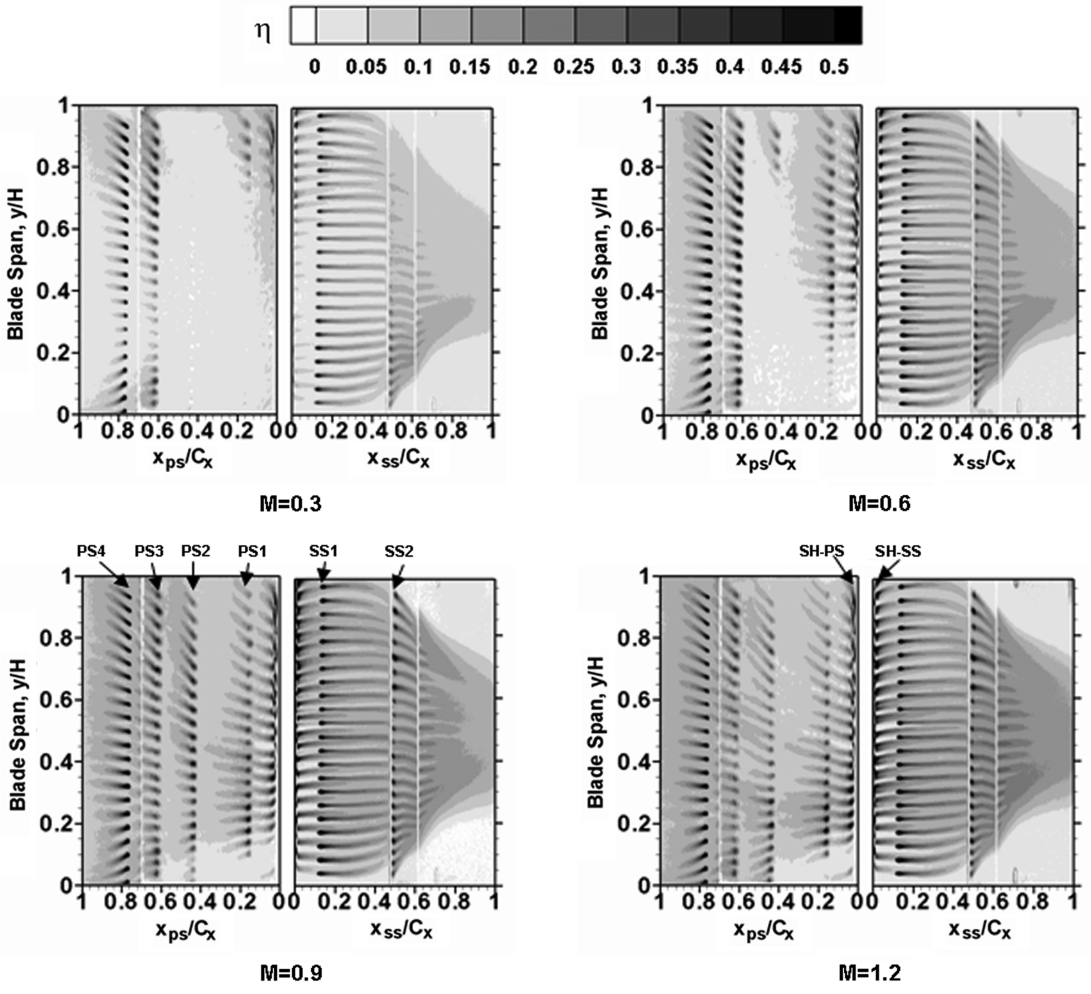

Fig. 10 Film-cooling effectiveness distribution with no wake.

pressure side holes and produce a relatively uniform coverage on the pressure surface. The film effectiveness on the pressure surface steadily increases when M varies from 0.3 to 0.9; whereas, the effectiveness enhancement is relatively insignificant when M changes from 0.9 to 1.2. Considering the SLA material durability at higher pressure, the current study did not go to a higher average blowing ratio. If M further increased (such as to $M = 1.5$), the film effectiveness on the pressure side might decrease due to jet liftoff at higher jet momentum. Gao et al. [17] showed that the best film-cooling effectiveness is obtained at an average blowing ratio between 0.6 and 1.2 for the case of pressure side injection only. At a higher average blowing ratio of 1.5, the effectiveness decreases because the coolant jets penetrate and mix with the mainstream. It should be noted that the average blowing ratio in [17] is equivalent to the row-based local blowing ratio of the current study. From Fig. 9, it can be predicted that the local blowing ratio on the pressure side would be much higher than 1.5 if the averaged blowing ratio further increased. The coolant jet may lift off from the pressure surface and leave the blade surface less protected. In addition, the engine efficiency will reduce by consuming a large amount of coolant. In general, the pressure side is difficult to film cool due to the concave geometry. The concave surface produces an adverse pressure gradient and flow deacceleration. These are unfavorable for the coolant to attach to the blade surface. The coolant jets tend to lift off from the pressure surface and rapidly mix in the mainstream, resulting in less coolant coverage area and lower effectiveness level. This is attested by the short coolant trace and low effectiveness magnitude from PS1 and PS2 where the blade has the largest curvature. However, the multiple rows of a film-cooling hole design provide a pressure side fairly uniform film-cooling effectiveness distribution at the moderate average blowing ratios of $M = 0.9$ and $M = 1.2$.

The film protection on the suction surface is better than the pressure surface with larger film coverage and higher effectiveness level. According to Goldstein et al. [1], one possible reason for improved performance by shaped holes is the "Coanda effect" that causes the jet to hug the surface. The Coanda effect is more likely to occur on a convex surface. Moreover, the suction side produces favorable pressure gradient and flow acceleration, making it easier for the coolant to stay close to the suction surface. In addition, it can be found in Fig. 9 that the local blowing ratios (for SH-SS, SS1, and SS2) on the suction side increase with the increasing of the average blowing ratio; however, they do not exceed one. A steady increase of the film-cooling effectiveness with the increasing of the blowing ratio is expected for the local blowing ratios in this range. It can be seen that the coolant trace from the showerhead rows becomes wider and longer, and the effectiveness level becomes higher as M increases. Furthermore, with the showerhead coolant accumulation, the increase of effectiveness with M is more significant for the suction side film cooling.

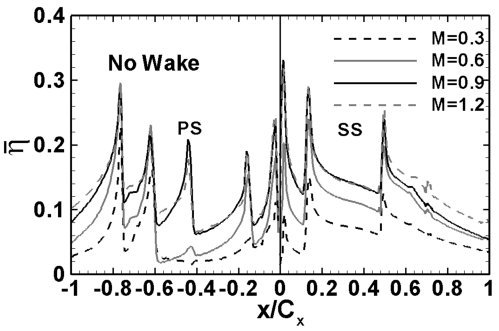

Fig. 11 Spanwise-averaged film-cooling effectiveness distributions with no wake.

Figure 11 shows the spanwise-averaged film-cooling effectiveness versus normalized axial chord length for the no-wake case. The location with a sharp increase of effectiveness corresponds to the film hole row location. In the range of study, the film effectiveness increases with the increasing of the average blowing ratio; however, the effectiveness on the pressure side decays faster than on the suction side. At $M = 0.3$ and $M = 0.6$, as discussed in the contour plots, the higher outer surface pressure prohibits the coolant ejecting from PS1 and PS2 holes, resulting in low effectiveness on the pressure side. Immediately downstream of the pressure side holes, the spanwise-averaged effectiveness $\bar{\eta}$ is quite similar for $M = 0.9$ and $M = 1.2$. Further downstream of the PS holes, $M = 1.2$ offers slightly higher $\bar{\eta}$ because more coolant is convected back to the surface. In general, the effectiveness for the downstream rows is higher than the upstream rows because more coolant is carried over from the upstream rows. This is particularly true for the suction side film-cooling rows. Although there were less number of film-cooling rows on the suction side, the $\bar{\eta}$ on the suction side seems comparable to that on the pressure side.

It can be seen from Fig. 10 that the coolant jets from the showerhead offer good film coverage in the leading region at higher average blowing rations. The coolant jets extend beyond the downstream PS1 and SS1 holes. This is more noticeable on the suction side at higher average blowing ratios. Figure 12 compares the spanwise-averaged film-cooling effectiveness for the cases with and without showerhead film cooling. With the showerhead coolant injection, the spanwise-averaged film-cooling effectiveness downstream of the PS1 row and SS1 row increases significantly. Further downstream, the effect of showerhead injection diminishes. The effect of showerhead injection is more profound at a higher averaged blowing ratio.

Narzary et al. [16] studied the film-cooling effectiveness with compound angle-shaped holes distributed on the pressure side and suction side. They also included the showerhead film cooling whose film-cooling hole design was identical to the current study. However, the shaped holes on the blade surface in their study were angled 45 deg (β) to the axial direction. The shaped hole expansion angles, hole locations, and flow conditions in their study were the same as the current study. To assess the effect of hole orientations, Fig. 13 shows the comparison of the spanwise-averaged effectiveness without upstream wake. In general, the compound angle-shaped holes provide higher film effectiveness than the axial-shaped hole.

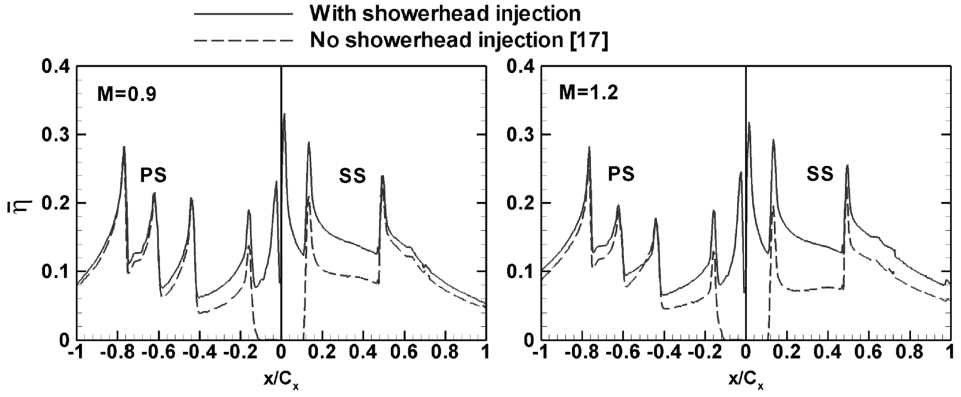

Fig. 12 Effect of showerhead injection with no wake.

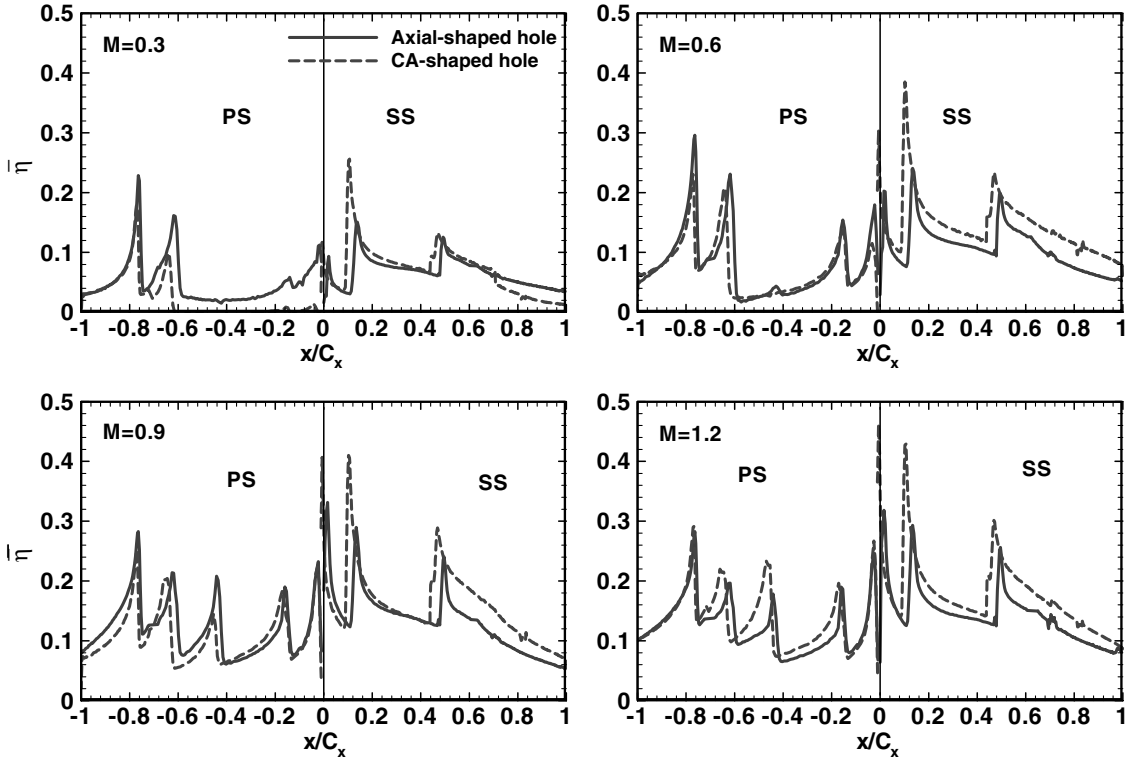

Fig. 13 Comparison of spanwise-averaged film effectiveness with no wake for axial-shaped holes and compound angle-shaped holes [16].

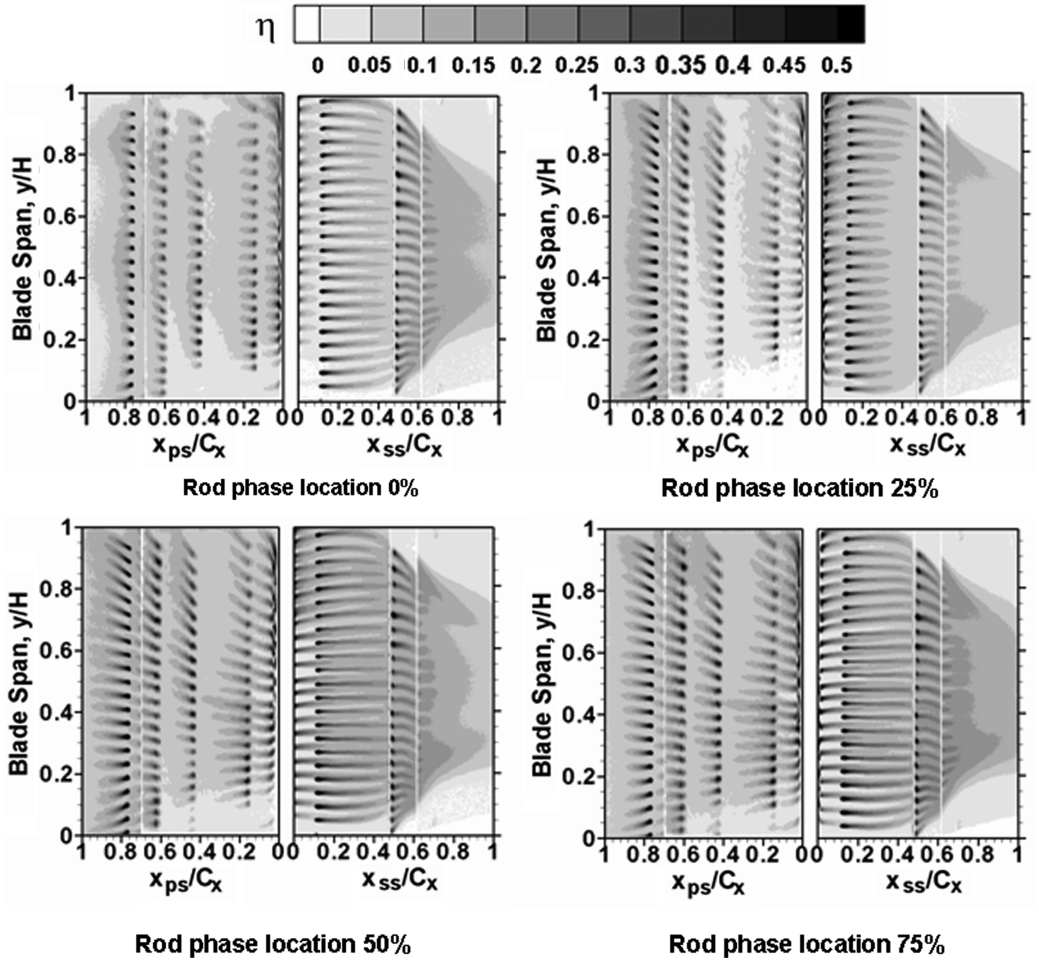

Fig. 14 Film-cooling effectiveness distributions at different rod positions ($M = 0.9$).

However, the advantage of compound angle holes on the pressure side is not as distinctive as on the suction side. As shown in Fig. 1, the higher effectiveness achieved by the compound angled holes mainly results from the wider film coverage due to jet deflection. The mainstream on the pressure side does not strictly follow the axial direction. The coolant jets from both the compound angle holes and the axial holes are deflected either toward the hub or toward the tip. This leads to comparable effectiveness on the pressure side at moderate average blowing ratios $M = 0.6$ and $M = 0.9$. The comparability on the pressure side changes a little at $M = 1.2$, at which the compound angle holes provide higher effectiveness than the axial hole. The compound angle holes have a bigger hole breakout area, and the jet penetration is reduced by the decreased jet momentum. However, the jet liftoff may occur to the axial holes with a smaller hole breakout area and higher jet momentum. The advantage of compound angle holes is more evident on the suction side film cooling except $M = 0.3$. The mainstream on the suction side fairly follows the axial direction except the tip and hub regions affected by the secondary vortices. Therefore, the coolant jets from compound angle-shaped holes are deflected by the mainstream, and cover a wider surface area. Whereas the coolant jets from axial-shaped holes follow the mainstream and the jet coverage is confined to the axial direction. In addition, the hole breakout area for the compound angle-shaped holes is larger than the axial-shaped hole. The jet momentum from those compound angle-shaped holes was further reduced. The coolant is prone to remain close to the surface with the reduced jet momentum. The coolant jet deflection and reduced jet momentum contribute to the higher effectiveness for the compound angle-shaped holes. However, the higher effectiveness for the compound angle-shaped holes may be accompanied by a higher heat transfer coefficient and larger losses due to coolant jets deflection and enhanced mixing with the mainstream. This research will continue to measure both heat transfer coefficient and losses on a gas turbine blade with the compound angle-shaped holes and axial-shaped holes.

To understand the nature of influence exerted by the wake rods at each phase location, the effectiveness distributions at four wake rod phases are presented in Fig. 14 for a typical average blowing ratio $M = 0.9$. In general, the presence of wake rods is detrimental to the film-cooling effectiveness as compared to the case of no wake. The vortex shedding from the wake rods brings additional turbulence in the mainstream, and the mixing between the coolant and the mainstream is enhanced. Therefore, the coolant traces become shorter and the effectiveness level becomes lower. The wake rod at phases 0 and 25% exhibits the more adverse effect compared to phases 50 and 75%. A conceptual view of the wake paths shown in Fig. 4 may help understand the wake effect. At phases 0 and 25%, the wakes are directed to the blade surface, so that the mixing between the coolant and the mainstream significantly increases. At phase 50%, the wakes generated by the rods mainly pass through the passage. At phase 75%, the wakes on the suction side passage are far away from the test blade, and the wakes on the pressure side passage are pushed away from the pressure side surfaces due to the high pressure on the pressure side. The wakes do not have a direct impact on the pressure side surface. Therefore both the 50 and 75% phases have less effect on the film cooling on the blade surface. Among the phases 0 and 25%, the phase 0% shows more detrimental effect on the pressure side, whereas phase 25% has more negative impact on the suction side. An interesting observation can be made by looking at the suction side effectiveness contours. It appears that the secondary vortices shield the coolant from SS2 row holes to some extent from the incoming mainstream. As a result, the coolant traces close to the tip and the hub regions propagate downstream in comparison to those near the midspan region.

Figure 15 shows the effectiveness distribution for blowing ratios $M = 0.6$ and $M = 1.2$ at rod phases 0 and 25%. It can be seen that the

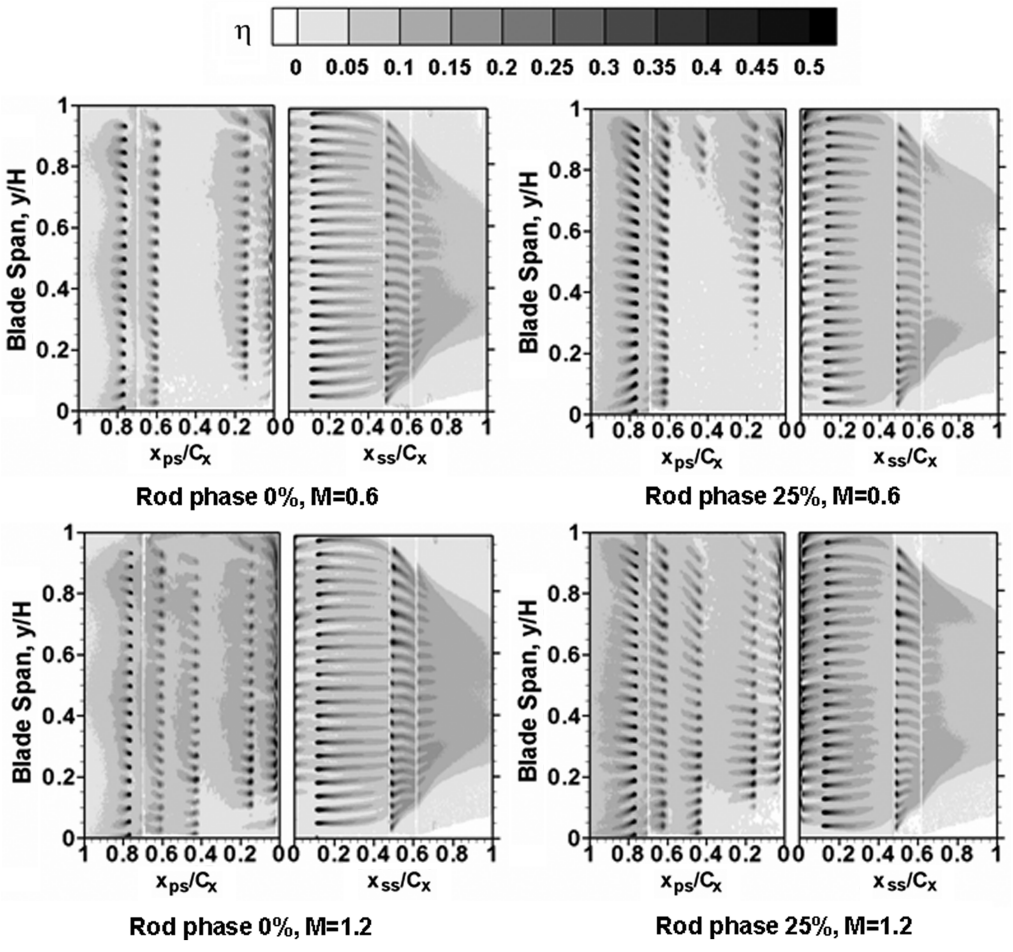

Fig. 15 Film-cooling effectiveness distribution at rod phase locations 0 and 25% for $M = 0.6$ and $M = 1.2$.

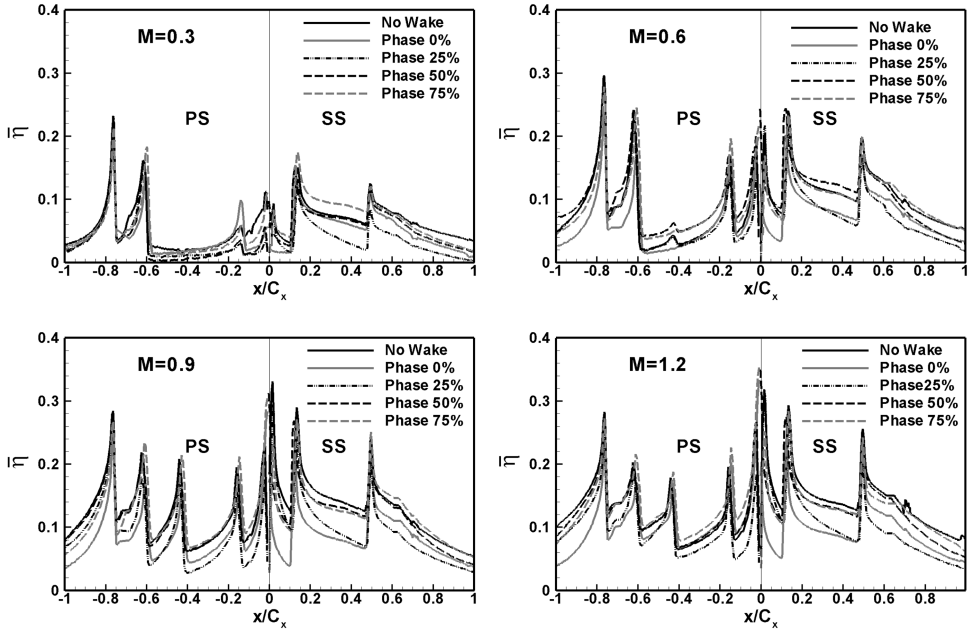

Fig. 16 Effect of stationary wake rods on spanwise-averaged film-cooling effectiveness.

effectiveness on the pressure side dramatically decreases at phase 0%. The enhanced mainstream turbulence produced by the wakes results in rapid mixing between the coolant and mainstream. The pressure surface is barely protected by the film cooling at this rod phase location. On the suction side, the film effectiveness degradation is more substantial at phase 25%. Not only is the elevated effectiveness reduced, but also the coolant trace is much shortened at rod phase location 25%. The secondary flow is predominant in the tip region and the hub region on the suction side. The wake effect is more pronounced in the midspan region of the suction side where the secondary vortices are negligible.

The effect of wake rod locations on the spanwise-averaged effectiveness is plotted in Fig. 16. Taking $M = 0.9$ as an example, $\bar{\eta}$ at rod phases 50 and 75% is slightly less than the case of no wake. However, more film effectiveness reduction is observed at rod phase locations of 0 and 25% as the coolant and mainstream interaction is enhanced due to wake impingement to the blade surface. The impact of wake for the other average blowing ratios is similar to $M = 0.9$ as the maximum detrimental effect takes place at rod phases 0 and 25%. The effect of the wake rod at $M = 0.3$ is not appreciable on the pressure side where the effectiveness is already low even without the wake.

Figure 17 shows the influence of the blowing ratio on the spanwise-averaged film-cooling effectiveness at the four wake rod locations. The blowing ratio effect for the case of wake basically follows the same trend as the baseline case without wake. Increasing the average blowing ratios, the film effectiveness increases. For all the wake rod phases, the lowest average blowing ratio $M = 0.3$ gives the lowest averaged effectiveness on both the pressure side and the suction side. From $M = 0.9$ to $M = 1.2$, the $\bar{\eta}$ on the suction side are comparable. Immediately downstream of the film-cooling holes on the pressure side, $\bar{\eta}$ is close to each other from $M = 0.6$ to $M = 0.9$. However, further downstream of the holes, a higher average blowing ratio shows better effectiveness as more coolant is pushed back to the surface.

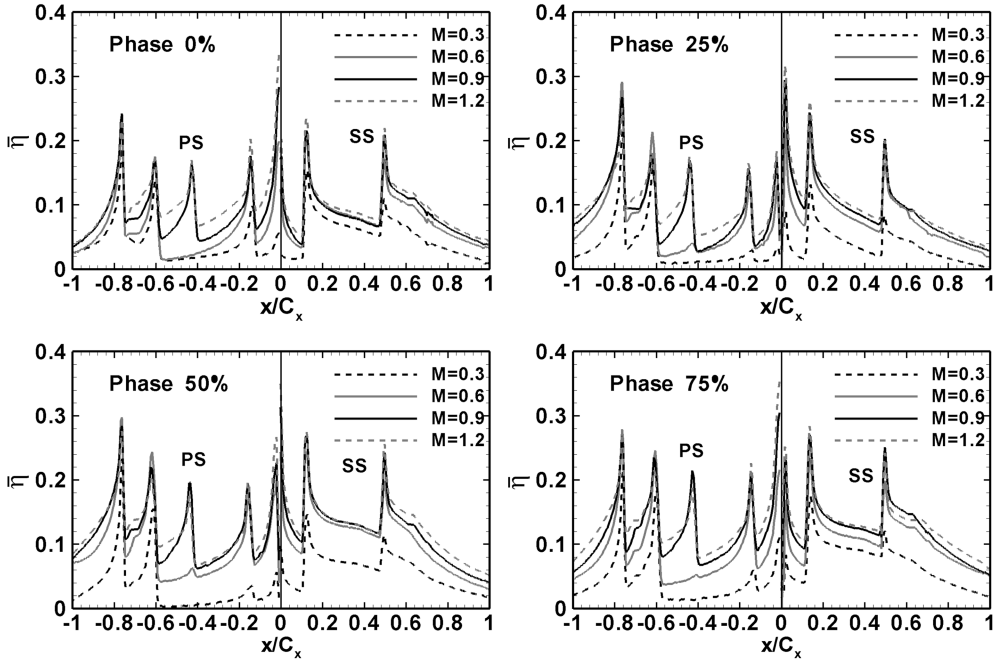

Fig. 17 Effect of blowing ratio on spanwise-averaged film-cooling effectiveness.

Conclusions

Experimental tests were performed on a fully cooled high pressure turbine rotor blade with radial angled cylindrical hole on the showerhead and axial laid-back fan-shaped holes on the blade surface. The shaped holes were featured with 10° expansion in the lateral direction and an additional 10° in the forward direction to the blade surface. The film-cooling effectiveness was measured using pressure sensitive paint (PSP) techniques. Some of the main findings from the present study are as follows:

1) For the film-cooling holes in shared cavities, the local blowing ratio distribution is highly dependent on the blade outer surface pressure and local mainstream velocity in the hole row location. When $M > 0.6$, the high local mainstream velocity results in a lower local blowing ratio for the holes in the suction side, although more coolant goes to the suction side where the static pressure is low. The extremely low local velocity in the stagnation region causes a very high local blowing ratio for the stagnation row in the showerhead region.

2) The coolant jets are deflected by the mainstream. On the pressure side, the coolant jet is deflected to either the tip or the hub depending on the hole location. On the suction side, the secondary vortices (tip leakage vortices and passage vortices, etc.) sweep the coolant to the midspan region and result in two uncooled triangular zones near the tip and the hub.

3) The film-cooling effectiveness increases with the increasing of the average blowing ratio in the range of study ($M = 0.3$–1.2). The convex surface on the suction side is favorable for the coolant jets to stay closer to the surface, whereas the concave surface on the pressure surface causes coolant jets separation from the pressure surface and rapid mixing with the mainstream. The effectiveness on the suction side is better than the pressure side with a higher effectiveness level and longer coolant trace.

4) The pressure side and the suction side film-cooling effectiveness is substantially increased by the showerhead film cooling.

5) An upstream wake can have a severe detrimental effect on film coverage depending on the wake rod phases. Phase locations of 0 and 25% significantly decrease the film-cooling effectiveness magnitudes. Wakes from 50 and 75% phase locations may not attach to the blade surfaces and hence do not impact the film-cooling effectiveness as much.

6) Compared with compound angle-shaped holes, the film-cooling effectiveness on the suction side is lower for the axial-shaped holes. The film effectiveness on the pressure side is comparable for the two hole configurations at moderate blowing ratios $M = 0.6$ and $M = 0.9$. At a relatively high average blowing ratio $M = 1.2$, the compound angled-shaped holes produce higher effectiveness.

Acknowledgment

This work has been funded through the Marcus Easterling Endowment Fund.

References

[1] Goldstein, R. J., Eckert, E. R. G., and Burggraf, F., "Effects of Hole Geometry and Density on Three-Dimensional Film Cooling," *International Journal of Heat and Mass Transfer*, Vol. 17, No. 5, 1974, pp. 595–607. doi:10.1016/0017-9310(74)90007-6

[2] Thole, K., Gritsch, M., Schulz, A., and Wittig, S., "Flowfield Measurements for Film Cooling Holes with Expanded Exits," ASME Paper 96-GT-174, 1996.

[3] Gritsch, M., Schulz, A., and Wittig, S., "Adiabatic Wall Effectiveness Measurements of Film-Cooling Holes with Expanded Exits," ASME Paper 97-GT-164, 1997.

[4] Yu, Y., Yen, C.-H., Shih, T. I.-P., Chyu, M. K., and Gogineni, S., "Film Cooling Effectiveness and Heat Transfer Coefficient Distributions Around Diffusion Shaped Holes," ASME Paper 99-GT-34, 1999.

[5] Schmidt, D. L., Sen, B., and Bogard, D. G., "Film Cooling with Compound Angle Holes: Adiabatic Effectiveness," ASME Paper 94-GT-312, 1994.

[6] Dittmar, J., Schulz, A., and Wittig, S. "Assessment of Various Film Cooling Configurations Including Shaped and Compound Angle Holes Based on Large Scale Experiments," ASME Paper GT-2002-30176, 2002.

[7] Chen, P. H., Hung, M. S., and Ding, P. P., "Film Cooling Performance on Curved Walls with Compound Angle Hole Configuration," *Annals of the New York Academy of Sciences*, Vol. 934, 2001, pp. 353–360.

[8] Teng, S., Han, J. C., and Poinsatte, P.E., "Effect of Film-Hole Shape on Turbine-Blade Film-Cooling Performance," *Journal of Thermophysics and Heat Transfer*, Vol. 15, No. 3, 2001, pp. 257–265.

[9] Teng, S., Sohn, D. K., and Han, J. C., "Unsteady Wake Effect on Film Temperature and Effectiveness Distributions for a Gas Turbine Blade," *Journal of Turbomachinery*, Vol. 122, No. 2, 2000, pp. 340–347. doi:10.1115/1.555457

[10] Ou, S., Han, J. C., Mehendale, A. B., and Lee, C. P., "Unsteady Wake over a Linear Turbine Blade Cascade with Air and CO2 Film Injection: Part 1—Effect on Heat Transfer Coefficients," *Journal of Turbomachinery*, Vol. 116, No. 4, 1994, pp. 721–729.

[11] Mehendale, A. B., Han, J. C., Ou, S., and Lee, C. P., "Unsteady Wake over a Linear Turbine Blade Cascade with Air and CO2 Film Injection: Part 2—Effect on Film Effectiveness and Heat Transfer Distributions,'' *Journal of Turbomachinery*, Vol. 116, No. 4, 1994, pp. 730–737.

[12] Du, H., Ekkad, S. V., and Han, J. C., "Effect of Unsteady Wake with Trailing Edge Ejection on Film Cooling Performance for a Gas Turbine Blade," *Journal of Turbomachinery*, Vol. 121, No. 3, 1999, pp. 448–455.

[13] Rigby, M. J., Johnson, A. B., and Oldfield, M. L. G., "Gas Turbine Rotor Blade Film Cooling with and Without Simulated NGV Shock Waves and Wakes," ASME Paper 90-GT-78, 1990.

[14] Heidmann, J. D., Lucci, B. L., and Reshotko, E., "An Experimental Study of the Effect of Wake Passing on Turbine Blade Film Cooling," *Journal of Turbomachinery*, Vol. 123, No. 2, 2001, pp. 214–221. doi:10.1115/1.1354621

[15] Mhetras, S., and Han, J. C., "Effect of Unsteady Wake on Full Coverage Film-Cooling Effectiveness for a Turbine Blade," AIAA Paper 2006-3403, May 2006.

[16] Narzary, D. P., Gao, Z., Mhetras, S., and Han, J. C., "Effect of Unsteady Wake on Film-Cooling Effectiveness Distribution on a Gas Turbine Blade with Compound Angle Shaped Holes," ASME Paper GT2007-27070, 2007.

[17] Gao, Z., Narzary, D. P., and Han, J. C., "Film Cooling on a Gas Turbine Blade Pressure Side or Suction Side with Axial Shaped Holes," *International Journal of Heat and Mass Transfer* (submitted for publication).

[18] McLachlan, B., and Bell, J., "Pressure-Sensitive Paint in Aerodynamic Testing," *Experimental Thermal and Fluid Science*, Vol. 10, No. 4, 1995, pp. 470–485. doi:10.1016/0894-1777(94)00123-P

[19] Wright, L. M., Gao, Z., Varvel, T. A., and Han, J. C., "Assessment of Steady State PSP, TSP and IR Measurement Techniques for Flat Plate Film Cooling," ASME Paper. HT-2005-72363, 2005.

[20] Coleman, H. W., and Steele, W. G., *Experimentation and Uncertainty Analysis for Engineers*, Wiley, New York, 1989, Chaps. 3, 4.

[21] Gritsch, M., Schulz, A., and Wittig, S., "Discharge Coefficient Measurements of Film-Cooling Holes with Expanded Exits," ASME Paper 97-GT-165, 1997.